Charmonium in medium: From correlators to experiment

Xingbo Zhao and Ralf Rapp
Cyclotron Institute and Physics Department, Texas A&M University, College Station, Texas 77843-3366, USA
(Received 1 September 2010; published 30 December 2010)

We set up a framework in which in-medium charmonium properties are constrained by thermal lattice quantum chromodynamics and subsequently implemented into a thermal rate equation enabling the comparison with experimental data in heavy-ion collisions. Specifically, we evaluate phenomenological consequences for charmonium production originating from two different scenarios in which either the free or the internal energy are identified with the in-medium two-body potential between charm and anticharm quarks. These two scenarios represent J/ψ "melting temperatures" of approximately $1.25T_c$ ("weak binding") and $2T_c$ ("strong binding"), respectively. Within current uncertainties in dissociation rates and charm-quark momentum spectra, both scenarios can reproduce the centrality dependence of inclusive J/ψ yields in nuclear collisions at the Super Proton Synchrotron (SPS) and the Relativistic Heavy-Ion Collider (RHIC) reasonably well. However, the "strong-binding" scenario associated with the internal energy as the potential tends to better reproduce current data on transverse momentum spectra at both SPS and RHIC.

DOI: 10.1103/PhysRevC.82.064905 PACS number(s): 25.75.−q, 12.38.Mh, 14.40.Pq

I. INTRODUCTION

Systematic studies of charmonium production in ultrarelativistic heavy-ion collisions (URHICs) are hoped to reveal the properties of charm-anticharm quark bound states in hot and dense matter. A central goal is to utilize these insights in the search for the quark-gluon plasma (QGP) and infer some of its basic properties, such as color screening, flavor transport, and the relevant degrees of freedom (see, e.g., Refs. [1–3] for recent reviews). To carry out this program quantitatively requires the combination of theoretical approaches to evaluate charmonium spectral functions in medium with phenomenological models furnishing a realistic context for computing observables. The former category includes first-principle lattice–quantum chromodynamics (lQCD) calculations [4–7] of charmonium correlation functions and heavy-quark (HQ) free energies, as well the recently revived potential models [8–15] to compute the charmonium spectrum in the QGP. In the latter category, kinetic rate equations, transport, and statistical models have been pursued [16–23]. However, there are currently rather few calculations with quantitative connections between these two categories (see, e.g., Ref. [24]). It is the purpose of the present paper to elaborate such connections.

The phenomenological building block in our work consists of a kinetic rate equation that accounts for charmonium dissociation and regeneration in a thermally expanding fireball. The in-medium charmonium properties figuring into the rate equation are inferred from spectral functions that are constrained by Euclidean correlators and HQ free energies computed in thermal lQCD. The spectral functions are adopted from a recent potential-model calculation using a thermodynamic T matrix [15] with HQ free (or internal) energies as in-medium driving kernel. From these spectral functions we extract in-medium binding energies and bound-state masses that determine the reaction rates and equilibrium limit for the rate equation. We explicitly verify that the "reconstructed" spectral functions yield Euclidean correlator ratios that vary little with temperature (say, within ±10%), as found in lQCD. In view of the ongoing debate as to whether the free or internal energy is a more suitable quantity to be identified with a HQ potential, we will explore both possibilities as supplied through the T-matrix calculations in Ref. [15]. As found there and in previous works [10,13], the free and internal energy may be considered as providing a lower and upper limit, respectively, on the dissociation temperatures of charmonia, which in the following we will refer to as weak- and strong-binding scenarios. We will elaborate the phenomenological consequences of both scenarios for charmonium observables in URHICs at the Super Proton Synchrotron (SPS) and at the Relativistic Heavy-Ion Collider (RHIC), including centrality, transverse-momentum (p_T), and rapidity (y) dependencies.

This paper is organized as follows: In Sec. II we examine the equilibrium properties of charmonia obtained from lQCD via the potential model and extract the key parameters needed for the kinetic approach of charmonium production in URHICs. In Sec. III we review the required ingredients of our previously constructed rate equation for calculating the inclusive yield as well as the transverse-momentum spectra of charmonia. In Sec. IV we compare our numerical results with experimental data at SPS and RHIC. We conclude and give an outlook in Sec. V.

II. EQUILIBRIUM PROPERTIES OF CHARMONIA

In this section we discuss the equilibrium properties of charmonia ($\Psi = J/\psi$, χ_c and ψ') in the QGP medium as calculated from lQCD and extract the temperature-dependent quantities needed in the kinetic approach. Specifically, these are the in-medium charm-quark and charmonium masses, m_c^* and m_Ψ, respectively, the charmonium dissociation rate $\Gamma_\Psi^{\rm diss}$, and the charmonium dissociation temperature $T_{\rm diss}^\Psi$. The latter defines the temperature above which regeneration is not operative (i.e., the gain term of the rate equation is set to zero). We define the binding energy as

$$\varepsilon_B(T) = 2m_c^*(T) - m_\Psi(T). \tag{1}$$

In Sec. II A we review basic relations between correlators and spectral functions and extract pertinent quantities from the T-matrix approach of Ref. [15]. In Sec. II B we detail our calculations of the charmonium dissociation widths, which we assume to equal the total width of the charmonium. In Sec. II C we combine the extracted quantities to "re-construct" charmonium spectral functions and evaluate corresponding Euclidean correlator ratios in light of lQCD results.

A. Euclidean correlators and potential model

Lattice QCD currently provides equilibrium properties of charmonium mainly in terms of two quantities:

(i) The free energy, $F_{Q\bar{Q}}(r;T)$, of a static pair of heavy quark and antiquark. This is the main input for recent potential models. It remains controversial to date whether the free energy, the internal energy,

$$U_{Q\bar{Q}}(r;T) = F_{Q\bar{Q}}(r;T) - T\frac{\partial F_{Q\bar{Q}}(r;T)}{\partial T}, \qquad (2)$$

or any combination thereof, should be identified with a static $Q\bar{Q}$ potential at finite temperature T. In this work we therefore study two scenarios where either $U_{Q\bar{Q}}$ or $F_{Q\bar{Q}}$ is used as potential $V_{Q\bar{Q}}$. Because the internal energy leads to stronger binding than the free energy, we refer to the former and latter as strong- and weak-binding scenario, respectively.

(ii) The two-point correlation function of a quarkonium current, j_α, with hadronic quantum number α,

$$G_\alpha(\tau,\vec{r}) = \langle\langle j_\alpha(\tau,\vec{r}) j_\alpha^\dagger(0,\vec{0})\rangle\rangle, \qquad (3)$$

computed as a function of imaginary (Euclidean) time τ (also called temporal correlator). The imaginary part of the Fourier transform of the correlation function, $G_\alpha(\tau,\vec{r})$, is commonly referred to as the spectral function,

$$\sigma_\alpha(\omega,p) = -\frac{1}{\pi}\mathrm{Im}G_\alpha(\omega,p), \qquad (4)$$

which is related to the temporal correlator via

$$G_\alpha(\tau,T) = \int_0^\infty d\omega\sigma_\alpha(\omega,T)K(\omega,\tau,T), \qquad (5)$$

with the finite-T kernel,

$$K(\omega,\tau,T) = \frac{\cosh[(\omega(\tau-1/2T)]}{\sinh[\omega/2T]}. \qquad (6)$$

Lattice QCD results for two-point correlation functions are usually normalized to a "reconstructed" correlator evaluated with the kernel at temperature T,

$$G_\alpha^{\mathrm{rec}}(\tau,T) = \int_0^\infty d\omega\sigma_\alpha(\omega,T^*)K(\omega,\tau,T), \qquad (7)$$

but with a spectral function at low temperature T^*, where no significant medium effects are expected. The correlator ratio,

$$R_\alpha(\tau,T) = G_\alpha(\tau,T)/G_\alpha^{\mathrm{rec}}(\tau,T), \qquad (8)$$

is then an indicator of medium effects in $G_\alpha(\tau,T)$ through deviations from one. Current lQCD calculations find that the correlator ratio $R_\alpha(\tau,T)$, in the pseudoscalar (η_c) and vector (J/ψ) channel are close to 1 (within ca. 10%) at temperatures up to 2–3 T_c [6,25,26]. In the P-wave channels (scalar and axial vector) the correlator ratios are substantially enhanced over 1 at large τ. This feature is believed to originate from "zero-mode" contributions (at $\omega = 0$) that are related to the scattering of a charm (or anticharm) quark, $c \to c$ (or $\bar{c} \to \bar{c}$), rather than to $c\bar{c}$ bound-state properties [27]. This interpretation is supported by studies of the τ derivative of P-wave correlator ratios, which exhibits a much smaller variation (in the limit that the zero-mode part is a δ function, $\sigma_{\mathrm{zm}}(\omega) \propto \delta(\omega)$, its contribution to the temporal correlator is a constant) [28,29].

In principle, the in-medium properties of charmonia, such as pole mass, in-medium width, and dissociation temperature, are fully encoded in their spectral function. However, the finite number of data points for the two-point correlator computed in lQCD severely hampers the inversion of the transform in Eq. (5), rendering the determination of the spectral function difficult. In fact, potential-model analyses have shown that the use of either the free *or* internal energy can lead to agreement with lQCD correlators, albeit with rather different underlying binding properties (and associated dissociation temperatures). In the present work we therefore adopt the following strategy: we first extract the charm-quark masses and charmonium pole mass from a potential model, allowing us to define the binding energy according to Eq. (1). The latter is an important ingredient in the quantitative evaluation of the Ψ dissociation rate [30], which will be done in the following section II B in a perturbative ("quasifree") approximation. We then "reconstruct" in-medium charmonium spectral functions using a relativistic Breit-Wigner + continuum ansatz, where the Ψ width and mass figure into the Breit-Wigner part whereas the continuum is determined by the open-charm threshold ($2m_c^*$). For a more realistic evaluation, we include pole-strength factor $Z_\Psi(T)$ for the Breit-Wigner strength and a nonperturbative rescattering enhancement in the continuum [11,13]. The vanishing of the pole-strength factor furthermore serves to estimate the dissociation temperature of the ground state in each channel.

For definiteness we employ the potential model of Ref. [15] where quarkonium spectral functions and correlators have been calculated in a thermodynamic T-matrix approach, consistent with vacuum spectroscopy and including relativistic corrections for a proper description of scattering states. The calculations in there have been carried out for both free and internal energies as potential, and for two different lQCD inputs [4,5]. In both cases (and for both potentials), an approximate constancy (within $\pm 15\%$) of the correlator ratios for pseudoscalar charmonium was found (see lower panels of Figs. 12 and 14 in Ref. [15]). We believe that these results provide a reasonable representation and bracket for potential-model results. In the present work we adopt the results for the lQCD input from Ref. [5]. In Fig. 1 the temperature-dependent charm-quark mass is displayed, which is identified with the asymptotic value of the HQ potential,

$$m_c^*(T) \equiv m_c^0 + V_{Q\bar{Q}}(r\to\infty;T)/2. \qquad (9)$$

The in-medium masses decrease with temperature appreciably, whereas the magnitude of $m_c^*(T)$ is significantly smaller in the weak-binding compared to the strong-binding scenario. As expected, the binding energies (plotted in Fig. 2) also decrease

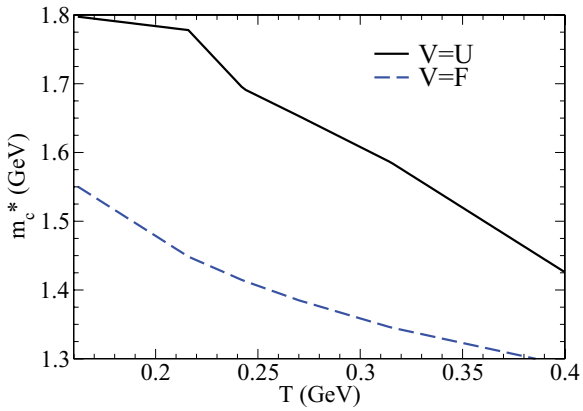

FIG. 1. (Color online) Temperature dependence of in-medium charm quark mass. The solid (dashed) line is for the strong (weak) binding scenario.

with T, again being significantly smaller in the weak-binding scenario. These features are, in fact, the main reason that both scenarios can be compatible with the small variations found in the lQCD correlator ratios: for weak or strong binding, a small or large constituent mass combines with a small or large binding energy, respectively, leading to an approximate compensation in the bound-state mass $m_\Psi(T)$, recall Eq. (1).

B. Dissociation rates

The inelastic dissociation rate of charmonia in the medium, $\Gamma_\Psi^{\rm diss}(T)$, plays a central role in URHIC phenomenology as it directly governs the time dependence of their abundance in an underlying rate equation [see, e.g., Eq. (23) in the following]. It contributes to the total width of the corresponding charmonium spectral function (in addition to elastic scattering which we neglect in the present work). However, it is currently not possible to quantitatively extract the width from temporal correlators [31]: for phenomenologically relevant values of the width of a few tens of MeV (or even up to 200 MeV) the correlator ratios are affected at a level of ∼5% [11,15] which is too small to be discerned from other uncertainties at this point. Furthermore, elastic and inelastic collisions contribute

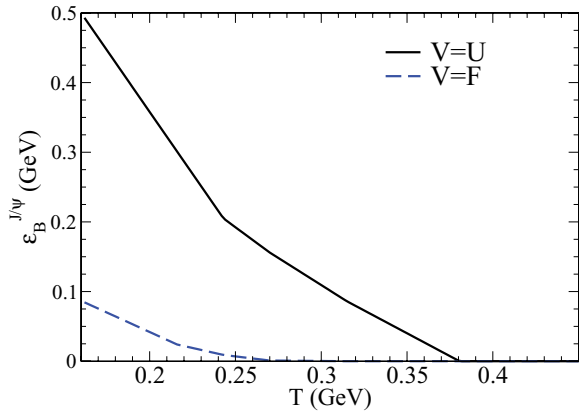

FIG. 2. (Color online) Temperature dependence of J/ψ binding energy. The solid (dashed) line is for the strong (weak) binding scenario with $V_{Q\bar{Q}}$=$U_{Q\bar{Q}}$($F_{Q\bar{Q}}$).

to the width with an a priori unknown partition (for relatively loosely bound states one expects the dissociation width to be dominant). In the present work we therefore calculate the dissociation rate based on perturbative QCD with an effective strong coupling constant which we later fine tune to reproduce the observed J/ψ suppression in central A-A collisions. The resulting value of α_s turns out to be ∼0.3, quite compatible with the short-distance (color-Coulomb) term in the effective potential used to extract the binding energies discussed in the previous section.

Let us briefly discuss basic mechanisms for charmonium dissociation in medium. In the QGP, the leading-order process is naively given by the gluo-dissociation process introduced more than 30 years ago [32], $\Psi + g \to c + \bar{c}$.[1] However, for small binding energies this process becomes inefficient (because of a shrinking phase space) and is superseded by inelastic reactions with an extra parton in the final state, $i + \Psi \to i + c + \bar{c}$ ($i = g, q, \bar{q}$) [30].[2] Following Ref. [30], we treat this process as a "quasielastic" collision between the parton i from the medium and the c or $\bar{c}$ quark in the bound state, $i + c' \to i + c$. In this quasifree approximation the charmonium dissociation cross section becomes twice the elastic cross section between the parton and the c quark, $\sigma_\Psi^{\rm diss} = 2\sigma_{ci}^{\rm el}$, as, for example, given in Ref. [33]. To account for the leading kinematic correction from the residual binding energy, the incoming parton needs to be energetic enough to break up the bound state, which sets a lower limit for the incoming parton momentum. Overall 4-momentum conservation for the process $i + \Psi \to i + c + \bar{c}$ is maintained by assigning the binding energy to a decrease in mass of the initial-state charm quark c' (i.e., $m_{c'} = m_c - \varepsilon_B$). In addition, we have introduced a Debye mass, $m_D = gT$, into the denominator of t-channel gluon-exchange propagator, $1/t \to 1/(t - m_D^2)$, to regulate the divergence for forward scattering (the strong coupling in m_D is taken consistently with the coupling constant α_s).

In the hadron gas (HG) phase, we employ a flavor-$SU(4)$ effective Lagrangian approach [34,35] to estimate the inelastic cross sections with π and ρ mesons. As we will see below most of the charmonium dissociation in the hot medium occurs in the QGP because the typical density of hadrons in HG is much smaller than that of partons in QGP, whereas the dissociation cross sections are of similar magnitude (around 1 mb).

The dissociation rate of a charmonium state at finite 3-momentum, p, can be obtained from the inelastic cross section by a convolution over the thermal distribution, $f^i(\omega; T)$, of medium particles in the QGP or HG,

$$\Gamma_\Psi^{\rm diss}(p, T) = \sum_i \int \frac{d^3k}{(2\pi)^3} f^i(\omega_k; T) \sigma_{\Psi i}^{\rm diss}(\vec{p}, \vec{k})\, v_{\rm rel}. \quad (10)$$

[1] In the language of effective field theory (EFT) [14], this corresponds to the color-singlet to color-octet transition, albeit final-state interactions in the $c + \bar{c}$ octet state are neglected here. However, they are repulsive and of order $\mathcal{O}(1/N_c^2)$ which renders them numerically very small.

[2] In EFT language, some of these processes (e.g., the ones involving t-channel gluon exchange between the thermal parton i and one of the charm quarks in the bound state) correspond to the Landau damping contribution to the width.

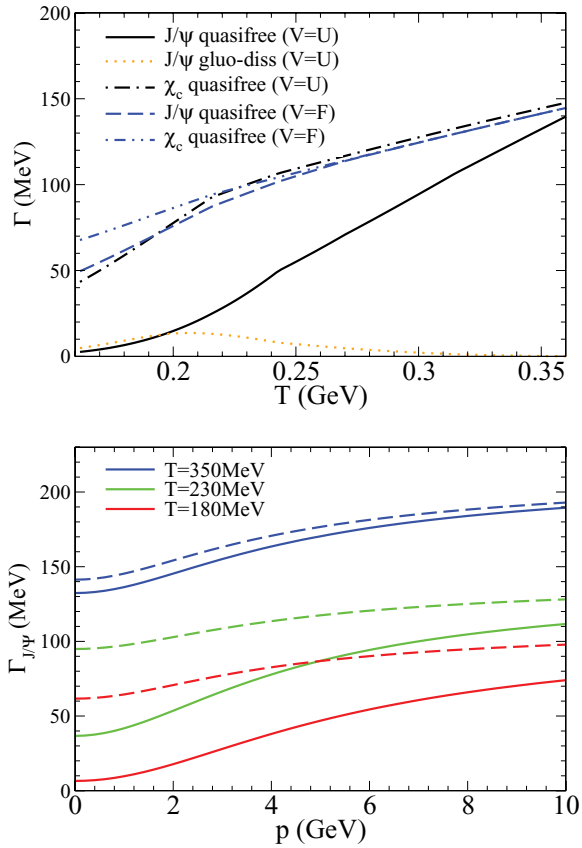

FIG. 3. (Color online) (Top panel) Temperature dependence of dissociation rates for J/ψ and χ_c calculated in quasifree approximation for the strong-binding (solid line, J/ψ; dot-dashed line, χ_c) and weak-binding scenarios (dashed line, J/ψ; dash-double-dotted line, χ_c). The dotted line indicates the contribution from J/ψ gluo-dissociation rate in the strong-binding scenario using $\alpha_s = 0.32$ in the underlying cross-section expression [32]. (Bottom panel) 3-momentum dependence of the J/ψ dissociation rate in the strong- and weak-binding scenarios (solid and dashed lines, respectively).

Here, $v_{\rm rel}$ is the relative velocity of Ψ and medium particle i. The temperature dependence of the quasifree dissociation rates for the J/ψ and χ_c in the QGP are plotted at $\vec{p} = 0$ versus T in the upper panel of Fig. 3, and for the J/ψ as a function of p at selected temperatures in the bottom panel. In the weak-binding scenario, there is rather little difference between the dissociation rates of J/ψ and χ_c, especially above $T = 200$ MeV. Only in the strong-binding scenario the larger J/ψ binding energy makes a large difference, suppressing its destruction by, for example, a factor of $\sim$5 at $T \simeq 200$ MeV relative to the χ_c and ψ' (not shown); this difference becomes larger (smaller) at smaller (larger) T. For comparison we also calculated the rate from the gluo-dissociation mechanism employing the expression derived in Ref. [32] with the same $\alpha_s = 0.32$ as in the quasifree rate and with ε_B obtained from the strong-binding scenario (note that the Coulombic binding is much smaller), which turns out to be inefficient for dissociating J/ψ's (and even more so for the excited states) and is thus neglected in the following. The 3-momentum dependence of the rates shows a monotonous increase with increasing p, which becomes more pronounced with increasing binding energy (for larger ε_B a finite 3-momentum facilitates the breakup because, on average, a larger center-of-mass energy is available in the collision of the bound state with thermal partons). This increase is a simple kinematic consequence of a monotonously increasing (or even constant) cross section with finite threshold and an increasing parton flux encountered by the moving J/ψ.

In the following section we determine the interplay of the charmonium widths with their binding energies extracted in the previous section to assess their survival in the QGP (e.g., as a resonance).

C. Spectral functions

We now turn to the construction of the charmonium spectral functions and the corresponding two-point correlation functions, and constrain the latter by lQCD computations. In doing so we introduce an additional quantity, namely the pole strength $Z_\Psi(T)$ of the Breit-Wigner bound-state part characterizing the disappearance of the state from the spectrum. The vanishing of $Z_\Psi(T)$ will be used to characterize the dissolution temperature above which regeneration in the rate equation is inoperative.

We first construct a model spectral function in vacuum, consisting of a zero-width bound state and a perturbative (leading order) continuum part,

$$\sigma_\Psi(\omega) = A_\Psi \delta(\omega - m_\Psi) + \frac{B_\Psi N_c}{8\pi^2}\Theta(\omega - s_0)\omega^2 \times \sqrt{1 - \frac{s_0^2}{\omega^2}}\left(a + b\frac{s_0^2}{\omega^2}\right). \quad (11)$$

Here, $N_c = 3$ is the number of colors and the coefficients $(a,b) = (1,-1), (2,1)$ characterize the scalar and vector channel, respectively [9]. The open-charm threshold in vacuum, s_0, is assumed to be given by twice the free D-meson mass, $s_0 \equiv 2m_D = 3.74$ GeV. The coefficient A is related to the overlap of the wave function, $R_{J/\psi}(0)$, or its derivative, $R'_{\chi_c}(0)$, at the origin [9,36],

$$A_{J/\psi} = \frac{3N_c}{2\pi}|R_{J/\psi}(0)|^2, \quad A_{\chi_c} = \frac{36N_c}{2\pi M_{\chi_c}^2}|R'_{\chi_c}(0)|^2. \quad (12)$$

These quantities can be estimated from the electromagnetic decay widths via [36]

$$\Gamma_{ee} = \frac{4e_Q^2\alpha^2 N_c}{3m_{J/\psi}^2}|R_{J/\psi}(0)|^2, \quad \Gamma_{\gamma\gamma} = \frac{144e_Q^4\alpha^2 N_c}{m_{\chi_c}^4}\left|R'_{\chi_c}(0)\right|^2, \quad (13)$$

where $\alpha = 1/137$ is the electromagnetic coupling constant and $e_Q = 2/3$ the charge of the charm quark (we use $\Gamma_{ee} = 5.55$ keV for the J/ψ and $\Gamma_{\gamma\gamma} = 2.40$ keV for the χ_{c0}). The resulting relations between A_Ψ and $\Gamma_{\Psi\to ee,\gamma\gamma}$ are

$$A_{J/\psi} = \frac{81m_{J/\psi}^2}{32\pi\alpha^2}\Gamma_{ee}, \quad A_{\chi_c} = \frac{81m_{\chi_{c0}}^2}{128\pi\alpha^2}\Gamma_{\gamma\gamma}. \quad (14)$$

The J/ψ and χ_{c0} masses are taken at their empirical vacuum values. The coefficient B_Ψ in the continuum part of Eq. (11)

equals one in the noninteracting limit. To account for rescattering, which is particularly important close to threshold, we scale it up to match the continuum as calculated from the vacuum T matrix in Ref. [15], amounting to $B_{J/\Psi} \simeq 2$ and $B_{\chi_c} \simeq 4$ in the vector and scalar channel, respectively. For simplicity we neglect ψ', χ_c' and higher excited states that play little role in the correlator ratios.

At finite temperature we replace the δ-function bound-state part by a relativistic Breit-Wigner (RBW) distribution while the continuum part is assumed to be of the same form as in the vacuum,

$$\sigma_\Psi(\omega) = A_\Psi Z_\Psi(T)\frac{2\omega}{\pi}\frac{\omega\Gamma_\Psi(T)}{\left(\omega^2 - m_\Psi^2(T)\right)^2 + \omega^2\Gamma_\Psi(T)^2} + \frac{B_\Psi N_c}{8\pi^2}\Theta(\omega - s(T))\omega^2\sqrt{1-\frac{s(T)^2}{\omega^2}} \times \left(a + b\frac{s(T)^2}{\omega^2}\right). \quad (15)$$

The in-medium continuum edge $s(T)$ is now taken as the charm-quark threshold at finite temperature, $s(T) \equiv 2m_c^*(T)$, consistent with the potential model; see Fig. 1. The RBW term includes the in-medium charmonium mass $m_\Psi(T)$ extracted from Eq. (1) based on Figs. 1 and 2, the width Γ_Ψ identified with the inelastic dissociation width discussed in the previous section, and the aforementioned pole-strength factor $Z_\Psi(T)$. The latter is adjusted to minimize the deviation of the correlator ratios from one. The resulting $Z_\Psi(T)$ for J/ψ (vector channel) is plotted in Fig. 4, from which we extract its dissociation temperature $T_{J/\psi}^{\rm diss} = 2.0(1.25)T_c$ in the strong (weak) binding scenario. Similar analysis in the scalar channel yields χ_c dissociation temperatures of $T_{\chi_c}^{\rm diss} = 1.3(1.0)T_c$ in the strong (weak) binding scenarios. We assume that χ_{c1} and χ_{c2} have the same dissociation temperatures as the χ_{c0}. For ψ' we simply assume its dissociation temperature to be T_c for both the strong- and weak-binding scenarios.

To comprehensively illustrate the medium effects we plot the final spectral functions for the vector channel in the strong- and weak-binding scenario in the QGP in Fig. 5, and their corresponding correlator ratios in Fig. 6; the spectral functions

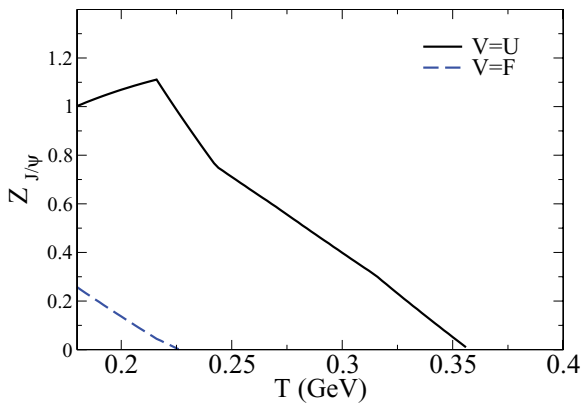

FIG. 4. (Color online) Temperature dependence of the strength of the resonance part of the S-wave spectral function $Z_\Psi(T)$. The solid (dashed) line is for the strong (weak) binding scenario.

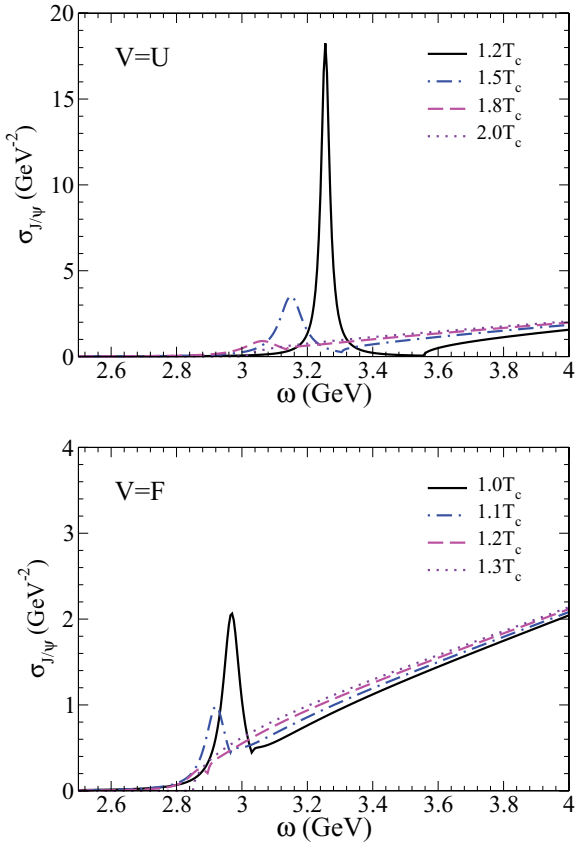

FIG. 5. (Color online) Spectral functions in the vector channel. The top (bottom) panel is for the strong (weak) binding scenario.

for the scalar channel are displayed in Fig. 7. We see that the correlator ratios are indeed close to one, as found in lQCD. In the hadronic phase (not shown), we assume vacuum masses for both charmonia and open-charm hadrons, which automatically ensures that the correlator ratios are close to one (deviations due to small charmonium widths in hadronic matter are negligible).

We are now in position to implement the in-medium properties of the charmonia into a kinetic rate equation in a thermal background, paving the way for applications to experimental data in heavy-ion collisions.

III. KINETIC APPROACH

The evolution of charmonium yields and spectra in a nucleus-nucleus (A-A) collision can be roughly divided into three stages. In the first, "primordial" stage (at small times $\tau \simeq 0$) charm-quark pairs are produced in initial hard nucleon-nucleon (N-N) collisions. In the second, "pre-equilibrium" stage ($0 \lesssim \tau \lesssim \tau_0$) charmonia are typically in the formation phase, but the so-called preresonance states are already subject to dissociation by passing-by nucleons. The third, "equilibrium" stage ($\tau \gtrsim \tau_0$) starts once the hot and dense medium has thermalized and lasts until thermal freeze-out after which hadrons stream freely to the detectors. During this stage charmonia are subject to dissociation by particles of the heat bath, but detailed balance requires that $c\bar{c}$ pairs in the medium

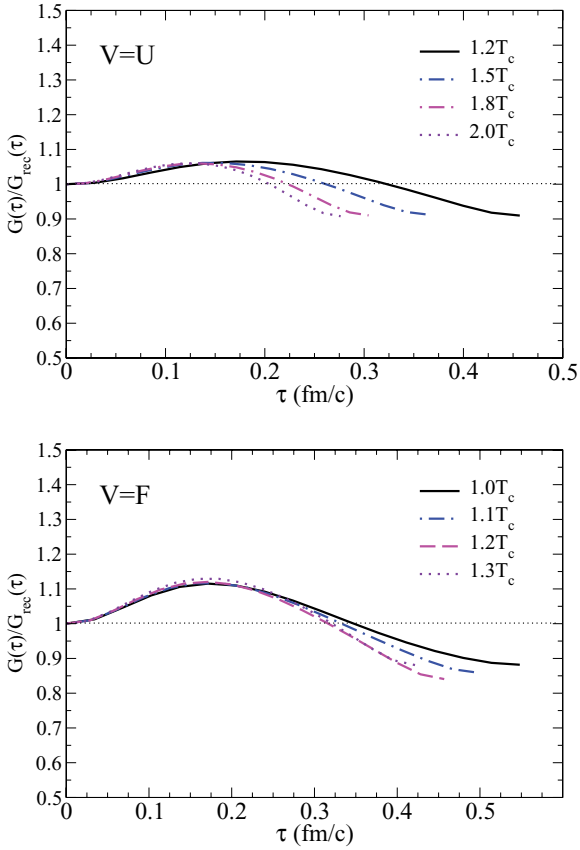

FIG. 6. (Color online) Ratio of vector channel correlator to the reconstructed correlator. The top (bottom) panel is for the strong (weak) binding scenario.

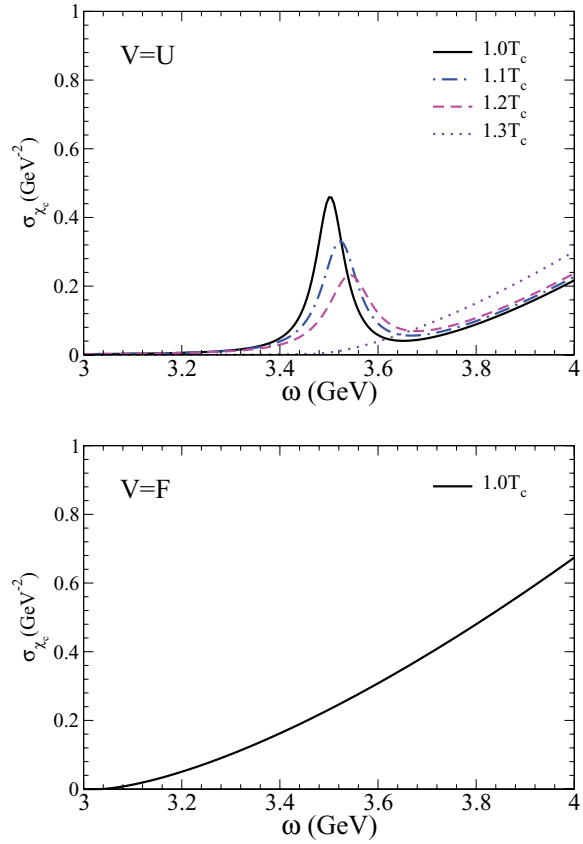

FIG. 7. (Color online) Spectral functions in the scalar channel. The top (bottom) panel is for the strong (weak) binding scenario. In the weak-binding scenario χ_{c0} has already melted at T_c.

can also recombine and "regenerate" charmonia (below their respective dissociation temperature).

Guided by the previous scheme, we have organized the remainder of this section as follows: In Sec. III A we discuss primordial charmonium production and its modifications in the pre-equilibrium stage, including rapidity and transverse-momentum dependencies. In Sec. III B we briefly recapitulate a simple fireball model that serves as a thermally evolving background for the charmonium rate equation. The latter is introduced in Sec. III C along with its main ingredients related to in-medium open-charm and charmonium properties. In Sec. III D we specifically address the transverse-momentum dependence of charmonium production in the equilibrium stage.

A. Cold nuclear matter effects

Charmonium production yields and p_t distributions following from the primordial and pre-equilibrium stage form the initial conditions for the thermal rate equation discussed in the next section. The starting point is primordial spectra based on experimental data in p-p collisions, modified by corrections specific to proton-nucleus (p-A) and extrapolated to A-A collisions. The corrections are commonly referred to as cold-nuclear-matter (CNM) effects, which include the following:

(i) Nuclear shadowing; The modification of the initial parton distribution functions in a nucleus relative to those in a proton, which affects both open and hidden charm yields in A-A relative to p-p collisions.
(ii) Cronin effect; The increase of the mean p_t of produced charmonia in A-A relative to p-p associated with initial-state parton scattering prior to the hard production.
(iii) Nuclear absorption; The dissociation of precharmonium states by passing-by nucleons.

In the present work, we assume a factorization of the charmonia phase-space distribution function into spatial and momentum parts,

$$f_\Psi(b, \vec{x}_t, \vec{p}_t, \tau_0) = f_\Psi(b, \vec{x}_t, \tau_0) f_\Psi(b, \vec{p}_t, \tau_0), \qquad (16)$$

(b is the impact parameter of the A-A collision, which we use as a measure of centrality equivalent to $N_{\rm part}$, the number of nucleon participants). The Cronin effect is readily implemented into the 3-momentum dependent part $f_\Psi(b, \vec{p}_t, \tau_0)$ via a Gaussian smearing of the charmonium p_t distribution in p-p collisions, $f_\Psi^{pp}(p_t)$,

$$f_\Psi(b, \vec{p}_t, \tau_0) = \int \frac{d^2q_t}{2\pi\langle\Delta p_t^2\rangle} \exp\left(-\frac{q_t^2}{2\langle\Delta p_t^2\rangle}\right) f_\Psi^{pp}(|\vec{p}_t - \vec{q}_t|). \qquad (17)$$

The nuclear increase of the average p_t^2, $\langle \Delta p_t^2 \rangle = \langle p_t^2 \rangle_{AA} - \langle p_t^2 \rangle_{pp}$, is estimated within a random-walk treatment of parton-nucleon collisions [37] as being proportional to the mean parton path length, $\langle l \rangle$, in the cold medium: $\langle \Delta p_t^2 \rangle = a_{gN} \langle l \rangle$. The coefficient a_{gN} is estimated from p-A data at SPS [38] and d-Au data at RHIC [39]. We use $a_{gN} = 0.076$ GeV^2/fm for $\sqrt{s} = 17.3$ AGeV Pb-Pb collisions and $a_{gN} = 0.1(0.2)$ GeV^2/fm for $\sqrt{s} = 200$ AGeV Au-Au collisions at mid- (forward) rapidity.

Nuclear absorption is evaluated within a Glauber model; the resulting charmonium distribution in the transverse plane takes the form,

$$f_\Psi(\vec{b}, \vec{x}_t, \tau_0) = \Delta y \frac{d\sigma_{pp}^\Psi}{dy} \int dz\, dz' \rho_A(\vec{x}_t, z)\, \rho_B(\vec{b} - \vec{x}_t, z') \times \exp\left\{ - \int_z^\infty dz_A \rho_A(\vec{x}_t, z_A) \sigma_{\rm abs} \right\} \times \exp\left\{ - \int_{z'}^\infty dz_B \rho_B(\vec{b} - \vec{x}_t, z_B) \sigma_{\rm abs} \right\}, \tag{18}$$

where $\rho_{A,B}$ are Woods-Saxon profiles [40] of nuclei A and B and $\Delta y = 1.8$ represents the rapidity coverage of our thermal fireball (see Sec. III B below). For the pp charmonium production cross per unit rapidity we take the values $d\sigma_{pp}^\Psi/dy = 37$ nb [41] for $\sqrt{s} = 17.3$ A GeV Pb-Pb [41] (with ca. 40% uncertainty) and $d\sigma_{pp}^\Psi/dy = 750(500)$ nb for $\sqrt{s} = 200$ AGeV Au-Au [42] at mid- (forward) rapidity (with ca. 10(20)% uncertainty). We utilize an effective Ψ-N absorption cross section $\sigma_{\rm abs}$ to parametrize both nuclear shadowing and absorption. Applying Eq. (18) to p-A collisions at SPS we obtain $\sigma_{\rm abs}^{J/\psi} = 7.3 \pm 1$ mb from the recent NA60 data at $E_{\rm lab} = 158$ GeV (corresponding to $\sqrt{s_{NN}} = 17.3$ GeV) [43]. The new experimental measurement at 158 GeV turns out to give a significantly larger value than previously available for 400-GeV proton projectiles, $\sigma_{\rm abs} \simeq 4.4$ mb [44] (the latter was confirmed by NA60 [43]), which was used in our previous calculations [21,23]. The comparison with recent PHENIX data [39,45] yields $\sigma_{\rm abs} \simeq 3.5$ mb (5.5 mb) for $\sqrt{s} = 200$ A GeV Au-Au collisions at midrapidity, $|y| < 0.35$ (forward rapidity, $|y| \in [1.2, 2.2]$). For simplicity, we assume the same absorption cross sections for the χ_c as for the J/ψ. However, for excited states $\sigma_{\rm abs}$ is expected to be significantly larger, even if they are not fully formed when the dissociation occurs. Taking guidance from the NA50 measurement with 400-GeV protons, we use $\sigma_{\rm abs}^{\psi'} \simeq 13$ mb at $\sqrt{s} = 17.3$ A GeV and $\sigma_{\rm abs}^{\psi'} \simeq 6.5(10)$ mb at $\sqrt{s} = 200$ A GeV for mid- (forward) y. For each charmonium state, the number surviving the pre-equilibrium stage in an A-A collision at impact parameter b thus amounts to

$$N_\Psi(b) = \int f_\Psi(\vec{b}, \vec{x}_t, \tau_0) d^2\vec{x}_t. \tag{19}$$

The rather pronounced rapidity dependence of $\sigma_{\rm abs}$ at RHIC casts doubt on interpreting this quantity as an actual absorption cross section. It seems more reasonable to associate its increase at forward y with nuclear shadowing [46] because the dissociation kinematics is very similar between mid- and forward rapidity. Although this does not affect the use of our "effective" $\sigma_{\rm abs}$, it does imply a nuclear shadowing effect on the open-charm cross section in A-A collisions (which is an important ingredient in the calculation of regeneration). As a "minimal" scheme we therefore associate the additional absorption of the J/ψ yield at forward y (relative to midrapidity) with a suppression of open-charm production caused by shadowing, whereas we assume no shadowing corrections at midrapidity. Thus, at both SPS and RHIC the number of primordially produced $c\bar{c}$ pairs at midrapidity is calculated from the pp cross section as

$$N_{c\bar{c}}^{\rm mid}(b) = \Delta y \left. \frac{d\sigma_{pp}^{c\bar{c}}}{dy} \right|_{y=0} T_{AB}(b), \tag{20}$$

whereas for forward y at RHIC we use

$$N_{c\bar{c}}^{\rm for}(b) = \Delta y \left. \frac{d\sigma_{pp}^{c\bar{c}}}{dy} \right|_{y=1.7} T_{AB}(b) \frac{S_{\rm nuc}^{\rm for}}{S_{\rm nuc}^{\rm mid}}. \tag{21}$$

Here, $T_{AB}(b)$ is the usual nuclear overlap function and $S_{\rm nuc}$ denotes the J/ψ suppression factor from CNM effects, parameterized by $\sigma_{\rm abs}$ in the Glauber formula, Eq. (18). In particular, the ratio $S_{\rm nuc}^{\rm for}/S_{\rm nuc}^{\rm mid}$ represents the extra suppression associated with nuclear shadowing, operative for both J/ψ and $c\bar{c}$ production. The input charm-quark cross section in pp is taken as $d\sigma_{\bar{c}c}/dy\ (y = 0) = 2.2\ \mu$b at SPS (according to the recent compilation of data in Ref. [47]), and as $d\sigma_{\bar{c}c}/dy\ (y = 0) = 123 \pm 40\ \mu$b at RHIC (in line with recent PHENIX measurements [48]). At forward rapidity we assume the pp charm-quark cross section to be reduced by 1/3 according to recent measurements [49].

B. Fireball model

Once the nuclear-collision system thermalizes, its temperature is the key quantity connecting to the in-medium properties of the charmonia as discussed in Sec. II. As in our previous work [21,23,30], we estimate the time evolution of the temperature using an isentropically and cylindrically expanding isotropic fireball characterized by an eigenvolume,

$$V_{\rm FB}(\tau) = \left(z_0 + v_z \tau + \tfrac{1}{2} a_z \tau^2\right) \pi \left(R_0 + \tfrac{1}{2} a_\perp \tau^2\right)^2. \tag{22}$$

The fireball expansion parameters v_z, a_z, $a_\perp$ are chosen such that the hadron spectra at thermal freeze-out are consistent with the empirically extracted light-hadron flow in resemblance of hydrodynamical calculations [we actually use a relativistic form of $a_\perp(\tau)$ that limits the surface speed, $v_s(\tau) = a_\perp \tau$, to below c]. The initial transverse radius R_0 represents the initial transverse overlap of the two colliding nuclei at a given impact parameter b, whereas the initial longitudinal length z_0 is related to thermalization time τ_0 through $z_0 \simeq \Delta y \tau_0$ where $\Delta y = 1.8$ represents the typical longitudinal rapidity coverage of a thermal fireball. We assume that at a formation time of $\tau_0 = 1.0(0.6)$ fm/c the medium at SPS (RHIC) first thermalizes with all the entropy $S_{\rm tot}(b)$ being built up. The latter is estimated from the multiplicities of observed charged particles

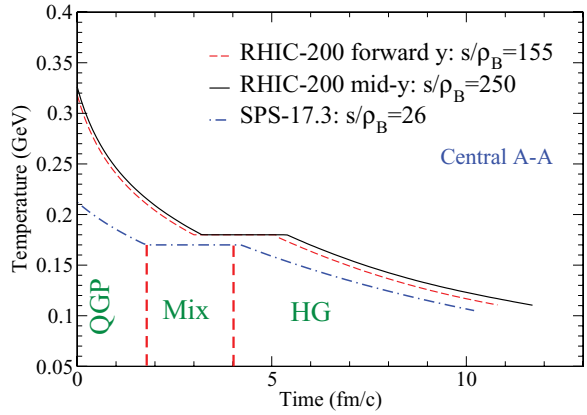

FIG. 8. (Color online) Time profiles of temperature for central collisions of heavy nuclei (participant number $N_{\rm part}$=380) at RHIC ($\sqrt{s} = 200$ AGeV; solid line, midrapidity; dashed line, forward rapidity) and SPS ($\sqrt{s} = 17.3$ AGeV; dot-dashed line).

and assumed to be conserved during the adiabatic expansion. We can then use the entropy density $s(\tau) = S_{\rm tot}/V_{\rm FB}$ at each moment τ in the evolution to infer the fireball temperature once we specify the equation of state of the medium, specifically $s(T)$. The QGP is modeled by an ideal gas of massive quarks and gluons whereas the hadronic phase is approximated by a noninteracting resonance gas with 76 mesonic and baryonic states up to masses of 2 GeV. The critical temperature $T_c = 170(180)$ MeV at SPS(RHIC) is roughly consistent with thermal-model fits to observed particle ratios [50] and predictions of lattice QCD [51]. A freeze-out temperature of $T_{\rm fo} \simeq 120$ MeV terminates the evolution and results in a total fireball lifetime of $\tau_{\rm fo} = 10$–12 fm/c for central A-A collisions. The resulting temperature evolution as a function of time τ is displayed in Fig. 8 for SPS and RHIC. Note that there is little difference between mid- ($|y| < 0.35$) and forward rapidity ($|y| \in [1.2, 2.2]$) for Au-Au collisions at RHIC because of the slowly varying rapidity density of charged particles over this y range [52] (cf. Ref. [53] for more details).

C. Rate equation in hot medium

We now proceed to the thermal rate equation to calculate the time dependence of the charmonium number N_Ψ throughout the third stage of the heavy-ion reaction,

$$\frac{dN_\Psi}{d\tau} = -\Gamma_\Psi^{\rm diss}(T)\big[N_\Psi - N_\Psi^{\rm eq}(T)\big]. \tag{23}$$

The rate equation is solved separately for $\Psi = J/\psi$, χ_c and ψ', with initial conditions given by Eq. (19). The loss term $-\Gamma_\Psi^{\rm diss} N_\Psi$ accounts for the dissociation of primordially produced charmonia and the gain term $\Gamma_\Psi^{\rm diss} N_\Psi^{\rm eq}$ for the regeneration of charmonia via coalescence of c and $\bar{c}$ quarks. Both processes are governed by the temperature-dependent inelastic reaction rate $\Gamma_\Psi^{\rm diss}(T)$, which is taken from Sec. II B [note that we do not employ the $p = 0$ value of the rate but rather a 3-momentum averaged value that is slightly larger; its precise value is obtained by matching the final yield of the loss term to the exact result obtained from solving the momentum-dependent Boltzmann equation (31) below]. The equilibrium limit of each charmonium state $N_\Psi^{\rm eq}(T)$ is intricately related to their equilibrium properties, which will be discussed further in the following. To make the decomposition of the J/ψ number at any time τ,

$$N_\Psi(\tau) = N_\Psi^{\rm prim}(\tau) + N_\Psi^{\rm reg}(\tau), \tag{24}$$

into (suppressed) primordial charmonia, $N_\Psi^{\rm prim}$, and regenerated ones, $N_\Psi^{\rm reg}(\tau)$, more explicit, we exploit the linearity of the rate equation (23). We define $N_\Psi^{\rm prim}(\tau)$ as the solution of the homogeneous rate equation,

$$\frac{dN_\Psi^{\rm prim}}{d\tau} = -\Gamma_\Psi^{\rm diss} N_\Psi^{\rm prim}, \tag{25}$$

with the same initial condition as for the full rate equation, $N_\Psi^{\rm prim}(0) = N_\Psi(0)$. The regeneration component $N_\Psi^{\rm reg}$ then follows as the difference between the solution of the full and the homogeneous rate equation, which can be expressed as

$$\frac{dN_\Psi^{\rm reg}}{d\tau} = -\Gamma_\Psi^{\rm diss}\big(N_\Psi^{\rm reg} - N_\Psi^{\rm eq}\big), \tag{26}$$

with vanishing initial condition $N_\Psi^{\rm reg}(\tau < \tau_0^\Psi) = 0$. The onset time of regeneration processes τ_0^Ψ is defined by $T(\tau_0^\Psi) = T_\Psi^{\rm diss}$ for each state Ψ.

Let us now return to the equilibrium limit of the charmonium abundances, $N_\Psi^{\rm eq}(T)$, which we evaluate within the statistical model. Because the thermal production and annihilation rates of $c\bar{c}$ are believed to be small at SPS and RHIC energies, $c\bar{c}$ pairs are assumed to be exclusively produced in primordial N-N collisions and conserved thereafter. The open and hidden charm states are then populated in relative chemical equilibrium according to the canonical charm-conservation equation,

$$N_{c\bar{c}} = \frac{1}{2} N_{\rm op} \frac{I_1(N_{\rm op})}{I_0(N_{\rm op})} + N_{\rm hid}, \tag{27}$$

where $N_{c\bar{c}}$ is the total number of charm-quark pairs from initial production; $N_{\rm op} = \gamma_c V_{\rm FB} n_{\rm op}$ is the total number of all open-charm states with pertinent equilibrium density $n_{\rm op}$; $N_{\rm hid} = \gamma_c^2 V_{\rm FB} n_{\rm hid}$ is the total number of all charmonium states with pertinent equilibrium density $n_{\rm hid}$; and γ_c is the charm-quark fugacity accounting for the deviation from chemical equilibrium with the heat bath ($\gamma_c = 1$ in full equilibrium). The ratio of modified Bessel functions, $I_1(N_{\rm op})/I_0(N_{\rm op})$, on the right-hand side of Eq. (27) is the characteristic canonical suppression factor that accounts for the exact conservation of net-charm number, $N_c - N_{\bar{c}}$, in each event [54,55]: for $N_{\rm op} \ll 1$, one has $I_1(N_{\rm op})/I_0(N_{\rm op}) \to \frac{1}{2} N_{\rm op}$, which acts as an additional (small) probability to enforce a vanishing net charm content in the system (i.e., both c and $\bar{c}$ have to be present simultaneously).

The open-charm number, $N_{\rm op}$, is evaluated as follows. For the QGP phase in the weak-binding scenario only charm quarks are counted as open-charm states. In the strong-binding scenario, the T-matrix calculations of Ref. [15] suggest that $c\bar{q}$ and $\bar{c}q$ (charm-light) bound states survive in QGP up to $\sim 1.3 T_c$; therefore, we count both charm quarks and the lowest-lying S-wave D mesons (D, D^*, D_s, and D_s^*) as open-charm states for $T < 1.3 T_c$. The charm-quark masses in the QGP correspond to the temperature-dependent ones displayed in Fig. 1, whereas for the meson resonances above

T_c we estimate from Ref. [15] $m_D = m_{D^*} \simeq 2.0$ GeV and $m_{D_s} = m_{D_s^*} \simeq 2.1$ GeV (hyperfine splitting was neglected). For the HG phase all charmed hadrons listed by the particle data group [56] are counted as open-charm states, with their vacuum masses. The hidden charm number $N_{\rm hid}$ is evaluated in line with the existing charmonium states and their masses at given temperature T, but its contribution to $N_{c\bar{c}}$ is numerically negligible.

Knowing $n_{\rm op}$, $n_{\rm hid}$, and $V_{\rm FB}$ at each temperature, one can solve Eq. (27) for the charm-quark fugacity $\gamma_c(T)$, and apply it to compute the statistical equilibrium limit of each charmonium state as

$$N_\Psi^{\rm stat} = \gamma_c^2 V_{\rm FB} n_\Psi, \tag{28}$$

in terms of its equilibrium density n_Ψ. In Fig. 9 we display the numerical results of the statistical equilibrium limit for J/ψ abundances (excluding feed-down) for central 200 A GeV Au-Au collisions at RHIC. The discontinuity at $1.3T_c$ for the strong-binding scenario (dot-dashed line) is from the inclusion of the D resonances in the QGP medium. We smoothly interpolate around the melting temperature for the D mesons with a hyperbolic tangent function (solid line) to represent a more gradual (dis)appearance of the D resonances (we have checked that this procedure has negligible impact on the calculation of observables in Sec. IV).

To achieve a more realistic implementation of the statistical equilibrium limit, we apply two corrections to $N_\Psi^{\rm stat}$ to schematically implement off-equilibrium effects of charm quarks in momentum and coordinate space. The former is aimed at simulating incomplete thermalization of the charm-quark p_t spectra throughout the course of the thermally evolving bulk medium. It is expected that the coalescence rate from non- or partially thermalized c- and $\bar{c}$-quark spectra is smaller than for fully thermalized ones [57,58], because the former are harder than the latter and thus provide less phase-space overlap for charmonium bound-state formation. We implement this correction by multiplying the charmonium abundances from the statistical model with a schematic relaxation factor [57],

$$N_\Psi^{\rm eq} = \mathcal{R}(\tau) N_\Psi^{\rm stat}, \quad \mathcal{R}(\tau) = 1 - \exp\left(-\tau/\tau_c^{\rm eq}\right), \tag{29}$$

where $\tau_c^{\rm eq}$ is a parameter that qualitatively represents the thermal relaxation time of charm quarks (it is one of our two main adjustable parameters in our phenomenological applications in Sec. IV). A rough estimate of this time scale may be obtained from microscopic calculations of this quantity within the same T-matrix approach as used here for charmonia, where the thermal charm-quark relaxation time turns out to be $\tau_{\rm eq}^c \simeq 3$–10 fm/c [15,59]. Such values allows for a fair description of open heavy-flavor suppression and elliptic flow at RHIC [59,60]. The second correction is applied in coordinate space, based on the realization that, after their pointlike production in hard N-N collisions, the c and $\bar{c}$ quarks only have a limited time to diffuse throughout the fireball volume. At RHIC and especially at SPS only few $c\bar{c}$ pairs are produced [e.g., $dN_{c\bar{c}}/dy \simeq 1.2$ in semicentral ($b = 7$ fm) Au-Au collisions at RHIC], and the hadronization time is smaller than the fireball radius. Thus, c and $\bar{c}$ will not be able to explore the full fireball volume but rather be restricted to a "correlation volume," $V_{\rm corr}$ [21,61] (the analogous concept was successfully applied to strangeness production in p-A and A-A collisions in the SPS energy regime [62]). We implement this correction by replacing the fireball volume $V_{\rm FB}$ in the argument of the Bessel functions in Eq. (27) by the correlation volume $V_{\rm corr}$ [21,24]. The latter is identified with the volume spanned by a receding $c\bar{c}$ pair,

$$V_{\rm corr}(\tau) = \frac{4\pi}{3}(r_0 + \langle v_c \rangle \tau)^3, \tag{30}$$

where $r_0 \simeq 1.2$ fm represents an initial radius characterizing the range of strong interactions, and $\langle v_c \rangle$ is an average speed with which the produced c and $\bar{c}$ quark recede from the production point; we estimate it from the average p_t in D-meson spectra in p-A collisions [21,63,64] as $\langle v_c \rangle \simeq 0.55(0.6)c$ at SPS (RHIC). The correlation volume leads to a significant increase of γ_c (because I_0/I_1 is reduced) and thus of the modified Ψ "equilibrium limit" due to an effectively larger $c\bar{c}$ density.

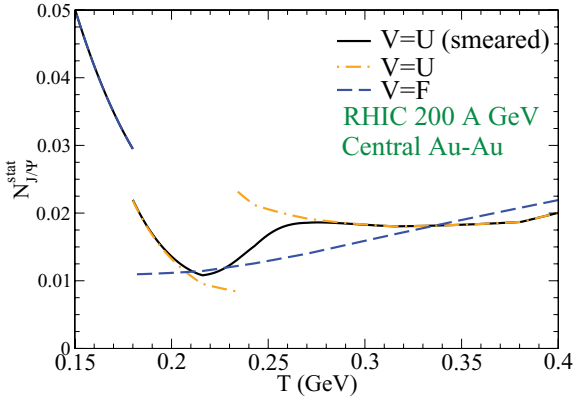

FIG. 9. (Color online) Temperature dependence of the in-medium J/ψ equilibrium limit using the statistical model in the QGP within the strong-binding scenario (dot-dashed lines, with and without D-meson resonances below and above $1.3\ T_c \simeq 234$ MeV, respectively; solid line, smooth interpolation of the previous two cases; see text for details), the weak-binding scenario (dashed line), and in the HG for temperatures below $T_c = 180$ MeV.

D. Transverse-momentum dependence

The transverse momentum dependence of in-medium charmonium production in A-A collisions was suggested as a tool to better discriminate primordial and regenerated production [30]. To investigate this observable within our approach we adopt the procedure suggested in Ref. [23] where the p_t spectra for the two components are evaluated at hadronization based on the decomposition given by Eqs. (24)–(26). For the primordial component we employ a more differential version of the rate equation (25) (i.e., a Boltzmann transport equation) to describe the evolution of the charmonium phase-space distribution functions, $f_\Psi(\vec{x}, \vec{p}, \tau)$, in a thermalized medium,

$$p^\mu\, \partial_\mu f_\Psi^{\rm prim}(\vec{x}, \vec{p}, \tau) = -E_\Psi \Gamma_\Psi^{\rm diss}(\vec{x}, \vec{p}, \tau) f_\Psi^{\rm prim}(\vec{x}, \vec{p}, \tau), \tag{31}$$

where $p_0 = E_\Psi = (m_\Psi^2 + \vec{p}^{\,2})^{1/2}$. The initial condition, $f_\Psi^{\rm prim}(\vec{x}, \vec{p}, \tau_0) = f_\Psi(\vec{x}, \tau_0) f_\Psi(\vec{p}, \tau_0)$, is still given as discussed in Sec. III A. As mentioned before, we neglect elastic charmonium rescattering, and consequently the modification of the charmonium p_t spectra in the thermal stage is mostly from the momentum dependence of the dissociation rates, $\Gamma_\Psi^{\rm diss}(\vec{x}, \vec{p}, \tau)$, given in Eq. (10) and plotted in the bottom panel of Fig. 3. We also account for "leakage" effects (i.e., charmonia escaping the fireball volume are no longer subject to suppression), which lead to the opposite trend compared to the increased suppression with p induced by the momentum dependence of the dissociation rate (charmonia with low p_t are more strongly suppressed because they stay longer within the fireball). At the moment of freeze-out, $\tau_{\rm fo}$, we obtain the final p_t spectra of the primordial component by integrating the spatial part of the solution of the Boltzmann equation,

$$\frac{dN_\Psi^{\rm prim}}{p_t dp_t} = 2\pi \int d^2x f_\Psi(\vec{x}, \vec{p}_t, \tau_{\rm fo}). \tag{32}$$

A microscopic evaluation of the momentum dependence of the regeneration component using the quasifree mechanism requires one to compute a 3-to-2 process, $i + c + \bar{c} \to i + \Psi$. In the framework of the Boltzmann equation, this is a rather involved calculation that will be reported in an upcoming publication [65]. For the time being, we approximate the p_t distributions of regenerated charmonia by local thermal distributions boosted by the transverse flow of the medium, amounting to a standard blast-wave description [66],

$$\frac{dN_\Psi^{\rm reg}}{p_t dp_t} \propto m_t \int_0^R r dr\, K_1\left(\frac{m_t \cosh y_t}{T}\right) I_0\left(\frac{p_t \sinh y_t}{T}\right), \tag{33}$$

($m_t = \sqrt{m_\Psi^2 + p_t^2}$). The medium is characterized by the transverse-flow rapidity $y_t = \tanh^{-1} v_t(r)$ using a linear flow profile $v_t(r) = v_s \frac{r}{R}$ with a surface velocity $v_s = a_\perp \tau_{\rm mix}$ and transverse fireball radius $R = R(\tau_{\rm mix})$ as given by the fireball expansion formula, Eq. (22), at the end of the mixed phase $\tau_{\rm mix}$. We evaluate the blast-wave expression at the hadronization transition (T_c) and neglect rescattering of Ψ's in the hadronic phase. Two additional effects are neglected in this treatment that to a certain extent tend to compensate each other: on the one hand, because of incomplete charm-quark thermalization, one expects the regenerated charmonium spectra to be harder than in equilibrium, but, on the other hand, a good part of the regeneration occurs before the mixed phase [22,67] (see also Fig. 14 later) so that the evaluation of the blast-wave expression at the end of the mixed phase presumably overestimates the blue shift from the flow field. An explicit evaluation of the gain term with realistic (time-dependent) charm-quark spectra within a Boltzmann transport equation [65] will be able to lift these approximations.

The total charmonium p_t spectra are the sum of the suppressed primordial and regenerated parts, Eqs. (32) and (33), with an absolute normalization following from the decomposition of the p_t-integrated rate equation, Eq. (24), at thermal freeze-out. The average p_t squared is readily computed as

$$\langle p_t^2 \rangle^{\rm prim,reg} = \frac{\int d^2p_t\, p_t^2 \frac{dN_\Psi^{\rm prim,reg}}{p_t dp_t}}{\int d^2p_t \frac{dN_\Psi^{\rm prim,reg}}{p_t dp_t}}, \tag{34}$$

which we compare to experimental data as part of the following section.

IV. COMPARISON TO SPS AND RHIC DATA

In this section we present and discuss the numerical applications of the previous framework to J/ψ data in URHICs at SPS and RHIC. For each observable, we confront the results of the strong- and weak-binding scenario in an attempt to discriminate qualitative features. The feed-down to J/ψ from χ_c and ψ' states is taken into account, assuming fractions of 32% and 8%, respectively, for primordial production in pp collisions. We have divided the discussion into the centrality dependence of inclusive J/ψ yields in Sec. IV A and their p_t dependence in Sec. IV B.

A. Centrality dependence of inclusive yields

The J/ψ yield in A-A collisions is usually quantified in terms of the nuclear modification factor as a function of centrality,

$$R_{AA}(b) = \frac{N_{J/\psi}^{AA}(b)}{N_{J/\psi}^{pp} N_{\rm coll}(b)}, \tag{35}$$

where $N_{\rm coll}(b)$ is the number of binary collisions of the incoming nucleons at impact parameter b. Before we turn to the results, we recall the two main parameters in our approach, which are the strong coupling constant α_s and the thermal charm-quark relaxation time $\tau_c^{\rm eq}$. The former controls the inelastic charmonium reaction rate and the latter the magnitude of the Ψ equilibrium limits. We adjust them to approximately reproduce the inclusive J/ψ yield for central A-A collisions at SPS and RHIC, within reasonable bounds. For α_s we find that a common value of 0.32, which is at the upper end of the value in the Coulomb term in the $Q\bar{Q}$ free energy, can be used, in combination with $\tau_c^{\rm eq} = 3.8$ fm/c for the strong-binding scenario and $\tau_c^{\rm eq} = 1.6$ fm/c for the weak-binding scenario. For simplicity, we refrain from introducing an additional temperature dependence into these parameters. The composition of the total yield, its centrality dependence, and p_t spectra can then be considered as a prediction within each of the two scenarios.

We begin with J/ψ production in $\sqrt{s} = 17.3$ AGeV Pb-Pb collisions at SPS, for which we compare our results in the strong- and weak-binding scenario with NA50 data in Fig. 10. For these data, the denominator in Eq. (35) is replaced by the number of Drell-Yan dileptons at high mass, whereas the numerator includes the branching ratio into dimuons. The pertinent proportionality factor, equivalent to the pp limit of this ratio (47.0 ± 1.4 [71]), and the CNM-induced suppression (dotted line in Fig. 10) are inferred from the latest NA60 p-A measurements [43], which we reproduce using

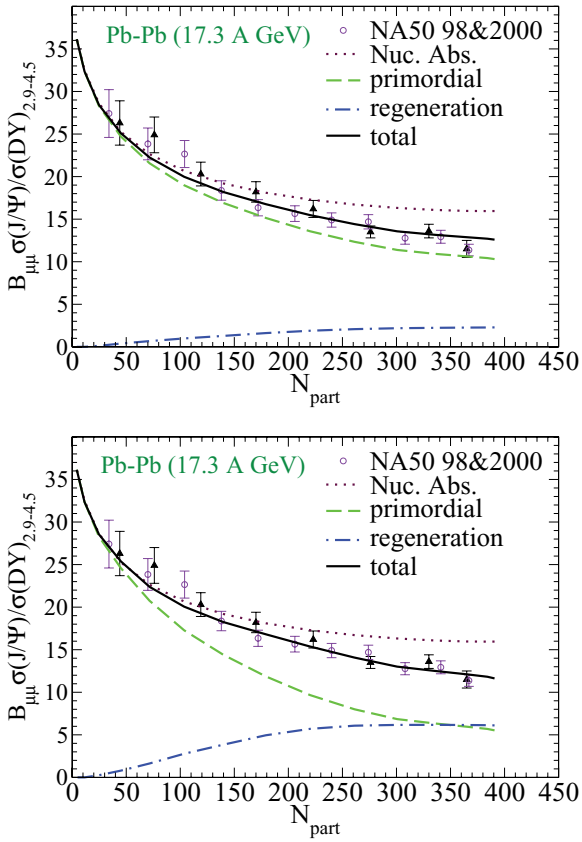

FIG. 10. (Color online) Results of the thermal rate-equation approach for J/ψ production (normalized to Drell-Yan pairs) versus centrality at SPS, compared to NA50 data [68,69]. Solid lines, total J/ψ yield; dashed lines, suppressed primordial production; dot-dashed lines, regeneration component; dotted lines, primordial production with CNM effects only. Top panel, strong-binding scenario; bottom panel, weak-binding scenario.

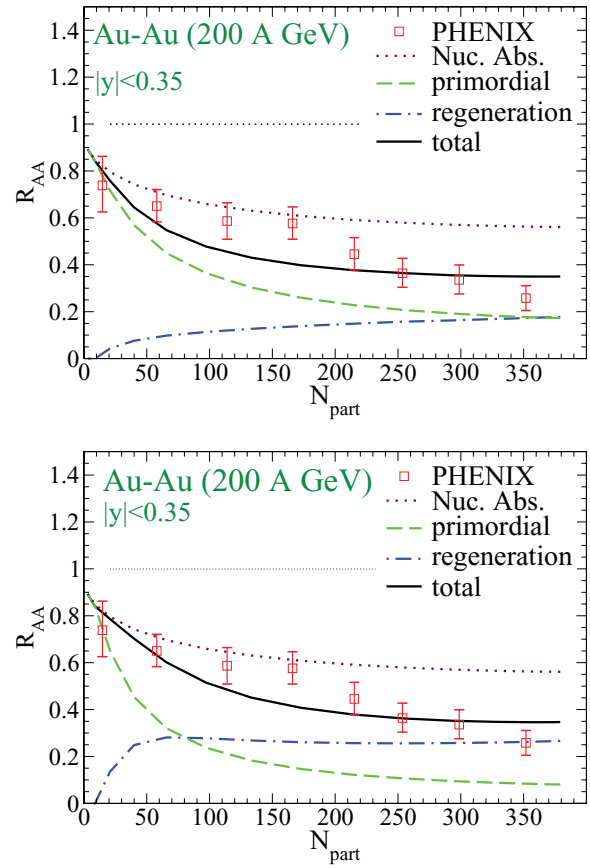

FIG. 11. (Color online) Results of the thermal rate-equation approach for the nuclear modification factor versus centrality at midrapidity at RHIC, compared to PHENIX data [70]. Solid lines, total J/ψ yield; dashed lines, suppressed primordial production; dot-dashed lines, regeneration component; dotted lines, primordial production with CNM effects only. Top panel, strong-binding scenario; bottom panel, weak-binding scenario.

the Glauber model formula, Eq. (18), with $\sigma_{\rm abs} = 7.3$ mb. The suppression of the primordial component (dashed line) relative to the nuclear absorption (dotted line) represents the "anomalous" suppression by the hot medium, which increases with centrality because of higher initial temperatures and longer fireball lifetimes. The regeneration component increases with centrality as well, mostly from the increase of the $\mathcal{R}$ factor and the larger lifetime that facilitates the approach to the equilibrium limit according to Eq. (26). According to detailed balance between dissociation and regeneration, an increase in the former also implies an increase in the latter. The sum (solid line) of primordial and regeneration contributions describes the centrality dependence of the inclusive J/ψ yield at SPS reasonably well in both scenarios. In the strong-binding scenario the primordial component is dominant and the majority of the anomalous suppression originates from the dissociation of χ_c and ψ', because at the temperatures realized at SPS ($T \simeq 200$ MeV) the quasifree dissociation rates for χ_c and ψ' are much larger than those for J/ψ; recall Fig. 3. In the weak-binding scenario, however, the regeneration yield becomes comparable to the primordial one for semicentral collisions due to larger dissociation rates and the smaller charm-quark equilibration time scale.

Next we examine the centrality dependence of J/ψ production in 200 AGeV Au-Au collisions at RHIC, first focusing on midrapidity ($|y| < 0.35$), as shown in Fig. 11. The suppression because of CNM effects (dotted line in Fig. 11) is inferred from the latest PHENIX d-Au measurements, which we reproduce using the Glauber model formula Eq. (18) with $\sigma_{\rm abs} = 3.5$ mb. For $N_{\rm part} \simeq 0 - 100$, the composition of primordial and regeneration contributions is quite comparable to the SPS for $N_{\rm part} \simeq 0 - 400$ within both scenarios. Beyond $N_{\rm part} \simeq 100$, suppression and regeneration continue to increase, leveling off at an approximately 50%–50% (20%–80%) partition for primordial and regeneration in the strong-binding (weak-binding) scenario in central collisions.

Let us now turn to J/ψ production at forward rapidity ($|y| \in [1.2,2.2]$) at RHIC, shown in Fig. 12. Again, both strong- and weak-binding scenarios reproduce the experimental data fairly well, with similar relative partitions for primordial and regeneration contributions as at midrapidity. However, one of

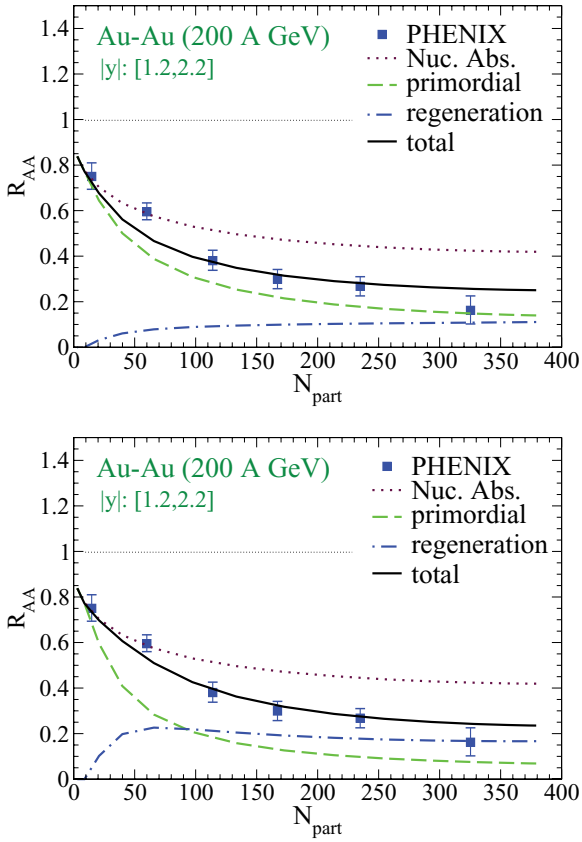

FIG. 12. (Color online) Results of the thermal rate-equation approach for the nuclear modification factor versus centrality at forward rapidity compared to PHENIX data [70]. Solid lines, total J/ψ yield; dashed lines, suppressed primordial production; dot-dashed lines, regeneration component; dotted lines, primordial production with CNM effects only. Top panel, strong-binding scenario; bottom panel, weak-binding scenario.

the "puzzles" about J/ψ production at RHIC is the fact that the total J/ψ yield is more strongly suppressed at forward rapidity than at midrapidity. In our approach this follows from the stronger shadowing at forward rapidity leading to less primordial production for both J/ψ and $c\bar{c}$ pairs. This leads to a reduction of both the primordial and regeneration J/ψ yields. Because the thermodynamic properties of the fireball are quite similar at mid- and forward rapidity (recall Fig. 8), charmonium suppression and regeneration in the hot medium are very similar as discussed in Ref. [53]. To quantify the difference we display the ratio between the corresponding R_{AA}'s in Fig. 13 for both scenarios, which clearly illustrates the importance of CNM effects to properly reproduce the data.

In Sec. II A we have argued that the strong- and weak-binding scenarios discussed here may be considered as limiting cases for J/ψ binding in the QGP, as bracketed by the identification of the heavy-quark internal and free energies with a Q-$\bar{Q}$ potential. From the results previously mentioned we believe that these scenarios also provide a reasonably model-independent bracket on the role of suppression and regeneration effects, in the following sense: At SPS, the strong-binding scenario defines a "minimal" amount of dissociation

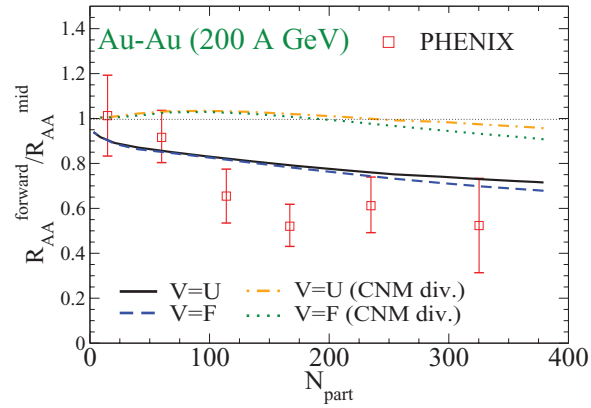

FIG. 13. (Color online) Results of the thermal rate-equation approach for the ratio of R_{AA} for J/ψ at forward and midrapidity versus $N_{\rm part}$ in strong (solid line) and weak (dashed line) binding scenarios compared to PHENIX data [70]. In the top two curves, CNM effects have been divided out in both numerator and denominator of the ratio.

required to provide the anomalous suppression beyond CNM effects (a small regeneration component is inevitable because of detailed balance). The application to RHIC energy then

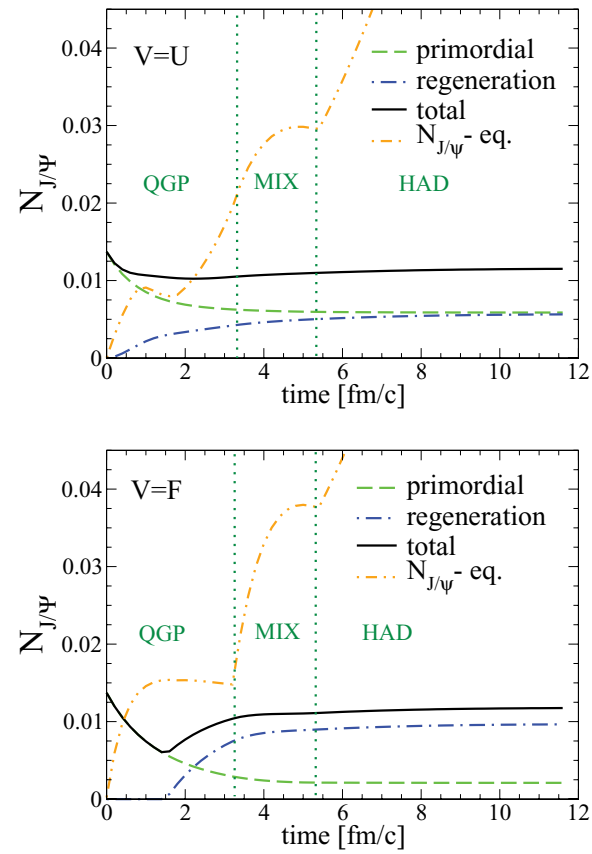

FIG. 14. (Color online) J/ψ abundance as a function of time in central ($N_{\rm part} = 380$) Au-Au collisions at RHIC. Solid lines, total; dashed line, primordial component; dot-dashed line, regeneration component; double dot-dashed line, equilibrium limit of J/ψ, $N^{\rm eq}_{J/\psi}$. Top panel, strong-binding scenario; bottom panel, weak-binding scenario.

implies an approximately equal partition of primordial and regenerated charmonia in central Au-Au, not unlike Ref. [22] where the vacuum charmonium binding energies ("strong binding") have been used in the QGP (together with the gluo-dissociation). On the other hand, in the weak-binding scenario, a large part of the J/ψ yield in central A-A is from regeneration even at SPS, limited by the constraint that for sufficiently peripheral collisions (and at sufficiently large p_t) a transition to primordial production compatible with p-A data should be restored. Clearly, for central A-A at RHIC (and certainly at LHC) the final yield is then dominated by regeneration. Because both scenarios describe the inclusive yields reasonably well, it is mandatory to investigate more differential observables to find discriminating evidence, which will be pursued in the following section.

It is instructive to examine the time evolution of J/ψ production in the two scenarios, displayed in Fig. 14 for central collisions at midrapidity at RHIC (excluding feed-down from χ_c and ψ'). In both scenarios most of the dissociation and regeneration occur in the QGP and the mixed phase because the HG reaction rates are small. In the weak-binding scenario the time-dependent J/ψ yield exhibits a "dip" structure around $\tau \simeq 1.5$ fm/c because the large dissociation rates suppress primordial J/ψ very rapidly and regeneration only starts after the medium temperature falls below the J/ψ dissociation temperature ($T_{J/\psi}^{\rm diss} \simeq 1.25 T_c$). This scenario thus is closest in spirit to the statistical hadronization model [19] where all initial charmonia are suppressed (or never form to begin with, except for corona effects) and are then produced at the hadronization transition.

B. Transverse-momentum spectra

The results of the previous section suggest that, within the current theoretical (e.g., charm-quark relaxation time $\tau_c^{\rm eq}$) and experimental uncertainties both of the "limiting" scenarios can reproduce the centrality dependence of the inclusive $R_{AA}^{J/\psi}(N_{\rm part})$ reasonably well at both SPS and RHIC energies. However, the composition between suppression and regeneration yields is rather different, which ought to provide a key to distinguish the two scenarios. The obvious "lever arm" are charmonium p_t spectra [30]. One expects that the primordial component is characterized by harder p_t spectra (following a power law at high p_t) while the regeneration component produces softer p_t spectra characterized by phase-space overlap of (partially) thermalized charm-quark spectra. However, in practice, the transition from the "soft" recombination regime to the "hard" primordial regime is quite uncertain; for example, collective flow and incomplete thermalization of c quarks can lead to a significant hardening of the regenerated J/ψ spectra, whereas a dissociation rate that increases with 3-momentum [23] can induce a softening of the spectra of the surviving primordial charmonia.

For a concise discussion of the p_t dependence of J/ψ as a function of centrality at SPS and RHIC we here focus on the average p_t^2, as compiled in Fig. 15. At the SPS (left panels), the centrality dependence of $\langle p_t^2 \rangle$ is largely dictated by the Cronin effect in the primordial component, especially in the strong-binding scenario where this contribution dominates the yield at all centralities. The momentum dependence of the dissociation rate induces a slight suppression of $\langle p_t^2 \rangle$ at large centrality compared to the case where only CNM effects are

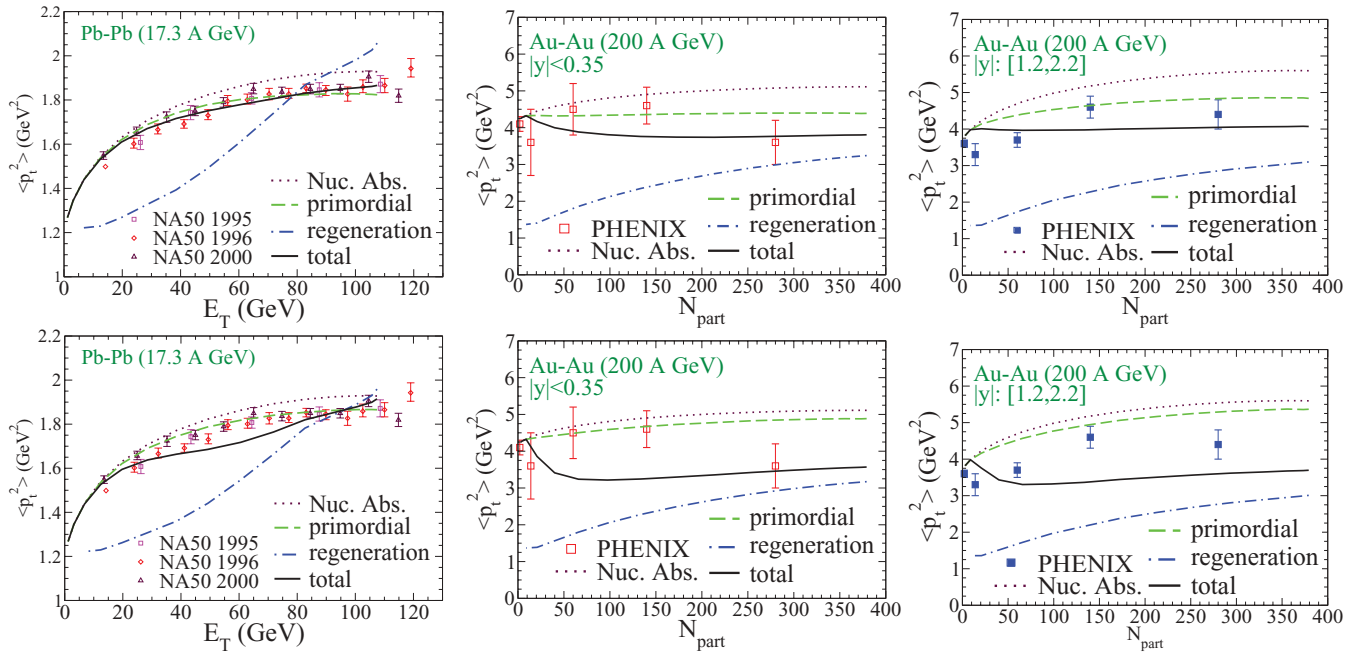

FIG. 15. (Color online) Results of the thermal rate-equation approach for $\langle p_t^2 \rangle$ versus centrality at SPS (left panels, compared to NA50 data [38,72]) and RHIC at mid- and forward rapidity (middle and right panels, respectively, compared to PHENIX data [70]). In each panel, $\langle p_t^2 \rangle$ is plotted for total J/ψ yield (primordial + regeneration component; solid lines), the suppressed primordial component (dashed line), the regeneration component (dash-dotted line), and primordial production with CNM effects only (dotted lines). The top (bottom) panels correspond to the strong-binding (weak-binding) scenario.

included (dashed versus dotted line) [23]. In the weak-binding scenario, larger contributions from regeneration induce a slight "dip" structure at intermediate centralities from a relatively small collective flow at the end of the (relatively short) mixed phase in these collisions.

At RHIC energy (middle and right panels of Fig. 15), the individual primordial and regeneration components show qualitatively similar behavior for $\langle p_t^2 \rangle (N_{\rm part})$ as at SPS (i.e., an increase from Cronin effect and collective flow, respectively). At midrapidity, the general trend is that with increasing centrality the growing regeneration contribution pulls down the average $\langle p_t^2 \rangle$, in qualitative agreement with the data. The curvature of the $\langle p_t^2 \rangle (N_{\rm part})$ dependence, which appears to be negative in the data, is not well reproduced, neither by the strong- nor by the weak-binding scenario, even though the deviations are smaller in the former. A more microscopic calculation of the gain term, together with more accurate estimates of the Cronin effect, are warranted to enable more definite conclusions. For both rapidity regions, the $\langle p_t^2 \rangle$ of the suppressed primordial component is slightly larger in the weak- than in the strong-binding scenario. This is caused by the stronger 3-momentum increase of the dissociation rate in the strong-binding scenario (recall bottom panel of Fig. 3).

The overall comparison to SPS and RHIC data for the p_t dependence of J/ψ's seems to indicate a slight preference for the strong-binding scenario. This is mostly derived from the observation that for peripheral collisions the experimentally observed $\langle p_t^2 \rangle$ essentially follows the extrapolation of the Cronin effect, suggesting J/ψ production of predominantly primordial origin (the collective flow imparted on the regeneration component appears to be too small at these centralities).

The average p_t^2 mostly characterizes the momentum dependence of charmonium production at low and moderate p_t where most of the yield is concentrated. Recent RHIC data [73,74] have triggered considerable interest in J/ψ production at high $p_t \simeq 5-10$ GeV which is expected to provide complementary information. It was found that the suppression in $R_{AA}^{J/\psi}(p_t \gtrsim 5\,{\rm GeV})$ in Cu-Cu collisions is reduced compared to the low-p_t region, with R_{AA} values of ~0.7–1 or even larger [74]. This is quite surprising in light of the light-hadron spectra measured thus far at RHIC, which all exhibit stronger suppression of $R_{AA} \simeq 0.25$ for $p_t \gtrsim 6$ GeV (even electron spectra from open heavy flavor, i.e., charm and bottom decays). It also appears to be at variance with the thermal J/ψ dissociation rates which, if anything, increase with momentum (recall Fig. 3) and thus imply a stronger suppression at higher p_t. Furthermore, the leakage effect referred to previously is not strong enough to produce the experimentally observed increase in $R_{AA}^{J/\psi}(p_T \gtrsim 5\,{\rm GeV})$ [23]. However, as was pointed out more than 20 years ago [75,76], the finite formation time of the charmonium states, in connection with Lorentz time dilation at high momentum, can lead to a reduction in the effective absorption cross section (or thermal rate) as long as the bound-state wave function has not developed (the preresonance state is more compact than the fully formed J/ψ). Furthermore, for high-p_t J/ψ spectra significant feed-down contributions from the decay of B mesons [77] are expected whose total yield is not suppressed. In Ref. [78] we have schematically implemented these effects

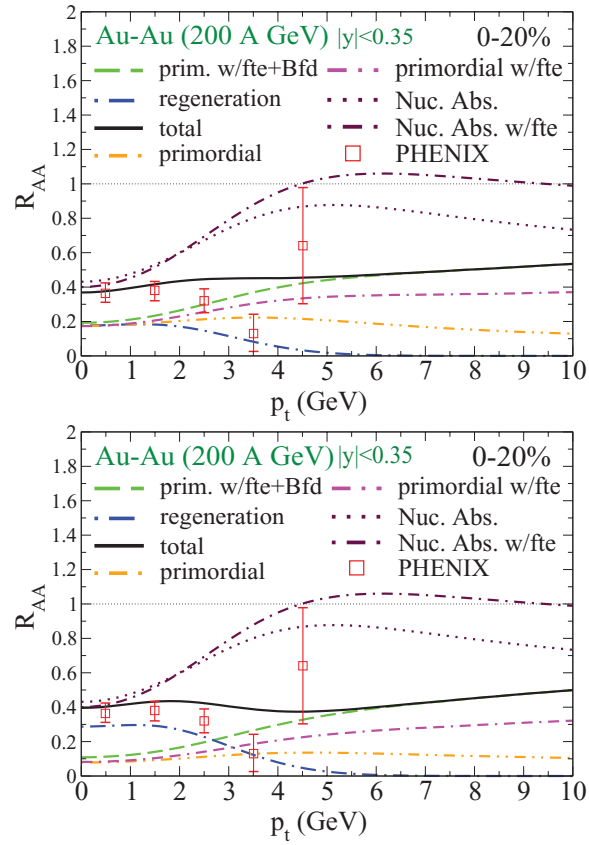

FIG. 16. (Color online) Nuclear modification factor for J/ψ p_t spectra in central 200 AGeV Au-Au collisions including formation-time effects (fte) and B-meson feed-down (Bfd) contributions. PHENIX data [70] are compared to our rate-equation calculations in the strong- and weak-binding scenarios (top and bottom panel, respectively).

into our rate-equation approach (as in the present paper) and found that $R_{AA}^{J/\psi}$ values of up to ~0.85 at $p_t \simeq 10$ GeV [78] can be recovered in Cu-Cu. Here, we extend these calculations to provide predictions for central Au-Au collision and specifically address the question of whether high-p_t J/ψ production can help to disentangle the strong- and weak-binding scenarios. Here we do not readjust any parameters relative to the previous calculation, which implies an increase of 15%–20% in the total yield. Our results for $R_{AA}^{J/\psi}(p_t)$ are displayed in Fig. 16 up to $p_t = 10$ GeV. We find that the suppression is reduced to about 0.5 at the highest p_t, compared to about 0.4 at low p_t. This is similar to the moderate enhancement found in the Cu-Cu case (where it went from ~0.65 to 0.85). More surprisingly, the high-p_t suppression is very similar in both strong- and weak-binding scenarios, despite the fact that the high-p_t yield is exclusively from the primordial component whose strength is very different in the two scenarios at low p_t. The reason is the 3-momentum dependence of the dissociation rates, which become quite similar in the two scenarios at large 3-momentum: at $p \simeq 10$ GeV, the difference in the energy threshold because of binding energies of several 100 MeV becomes less relevant so that a collision with almost any thermal parton is energetic enough for dissociating the bound state.

Let us finally comment on the elliptic flow, $v_2(p_t)$, of the J/ψ, which was hoped to be another good discriminator of primordial and regenerated production. For the former, a nonzero v_2 is basically from the path-length difference when traversing the azimuthally asymmetric fireball, typically not exceeding 2%–3%. For the latter, much larger values can be obtained if the coalescing charm quarks are close to thermalized. However, as pointed out in Ref. [78], the well-known mass effect suppresses the $v_2(p_t)$ for heavy particles at $p_t \lesssim m$; it is precisely in this momentum regime where the regeneration component is prominent. Thus, we predict that in both strong- and weak-binding scenarios the total J/ψ $v_2(p_t)$ does not exceed ~3% at any p_t. The only alternative option we can envision is strong elastic interactions of the J/ψ, which is only conceivable in the strong-binding scenario to avoid breakup in scattering off thermal partons [64].

V. CONCLUSION

The main goal of this work was to construct charmonium spectral functions that are constrained by thermal lattice-QCD computations, and to apply them to experimental data in heavy-ion collisions. Employing a thermal rate equation we have implemented equilibrium properties of charmonia (binding energy, constituent charm-quark mass, and dissociation rate) as extracted from a thermodynamic T-matrix calculation. The resulting spectral functions for two "limiting" scenarios, with small and large J/ψ dissociation temperatures, have been verified to produce a weak temperature dependence in pertinent Euclidean correlators, roughly compatible with lQCD. We have argued that these two scenarios may serve as generic representatives for charmonium kinetics in heavy-ion collisions, bracketing strong and weak in-medium binding. Therefore, we believe that the qualitative conclusions drawn from these two scenarios should be rather model independent. Within current theoretical uncertainties (especially for the degree of charm-quark relaxation and its impact on the J/ψ regeneration yield) and using essentially two fit parameters (τ_c and α_s controlling the regeneration yield and suppression strength) both scenarios can reproduce SPS and RHIC data for the centrality dependence of inclusive J/ψ production reasonably well. However, the partition of primordial and regenerated yields is quite different in the two scenarios: the former dominates for strong binding (down to 50% in central Au-Au at RHIC), whereas for weak binding regeneration largely prevails at RHIC energies (except for peripheral collisions). We have investigated the p_t dependence of the J/ψ yield in both scenarios and found that differences in the average p_t^2 reach up to 20% in semicentral Au-Au collisions. The strong-binding scenario seems slightly favored in this observable, but theoretical uncertainties (e.g., the blast-wave treatment of the regeneration component) prevent us from definite conclusions at this point. We also have to await more accurate A-A and p(d)-A data, where the latter determine the input in terms of shadowing, nuclear absorption, and Cronin effects.

Further developments of the theoretical approach are in order, and we plan to improve our calculations in several respects. First, as mentioned before, work is in progress employing a Boltzmann transport equation (31) extended by a microscopic treatment of the gain term to treat charmonia regeneration and dissociation on the same footing. This will enable an explicit account of (time-dependent) charm-quark phase-space distribution in c-$\bar{c}$ recombination reactions, as following, for example, from realistic Langevin simulations [59] with constraints from the T-matrix formalism and from open-charm observables. Second, hydrodynamic simulations of the medium evolution could be employed for a more detailed and realistic description of the temperature and the flow field of the underlying medium, especially in coordinate space. Third, a microscopic model for primordial $c\bar{c}$ and charmonium production is warranted to better disentangle nuclear shadowing and absorption in the pre-equilibrium stage, including formation-time effects. This would improve the initial conditions to the kinetic approach in the hot medium. These developments will eventually produce a comprehensive approach that can serve as a quantitative bridge between theoretical studies of charmonia in the QGP (and HG) and their phenomenology in heavy-ion collisions. As our investigations in the present paper have shown, quantitative studies at the 10%–20% level are needed to deduce basic properties of the strong force (such as color screening of Coulomb and confining interactions) from heavy-ion collisions. These insights are also pivotal to improve our knowledge of the phase structure of hot and dense QCD matter.

ACKNOWLEDGMENTS

We are grateful to L. Grandchamp for providing us with his codes. We thank A. Frawley and F. Riek for useful discussions. This work is supported by the US National Science Foundation (NSF) CAREER program under Grant No. PHY-0449489, by NSF Grant No. PHY-0969394, and by the A.-v.-Humboldt Foundation (Germany).

[1] R. Rapp, D. Blaschke, and P. Crochet, Prog. Part. Nucl. Phys. **65**, 209 (2010).
[2] L. Kluberg and H. Satz, arXiv:0901.3831 [hep-ph].
[3] P. Braun-Munzinger and J. Stachel, arXiv:0901.2500 [nucl-th].
[4] O. Kaczmarek, PoS C **POD07**, 043 (2007).
[5] P. Petreczky and K. Petrov, Phys. Rev. D **70**, 054503 (2004).
[6] G. Aarts, C. Allton, M. B. Oktay, M. Peardon, and J. I. Skullerud, Phys. Rev. D **76**, 094513 (2007).
[7] M. Asakawa, Nucl. Phys. A **783**, 269 (2007).
[8] F. Karsch, M. T. Mehr, and H. Satz, Z. Phys. C **37**, 617 (1988).
[9] A. Mocsy and P. Petreczky, Phys. Rev. D **73**, 074007 (2006).
[10] C. Y. Wong and H. W. Crater, Phys. Rev. D **75**, 034505 (2007).
[11] D. Cabrera and R. Rapp, Phys. Rev. D **76**, 114506 (2007).
[12] W. M. Alberico, A. Beraudo, A. De Pace, and A. Molinari, Phys. Rev. D **75**, 074009 (2007).
[13] A. Mocsy and P. Petreczky, Phys. Rev. D **77**, 014501 (2008).
[14] N. Brambilla, J. Ghiglieri, A. Vairo, and P. Petreczky, Phys. Rev. D **78**, 014017 (2008).
[15] F. Riek and R. Rapp, Phys. Rev. C **82**, 035201 (2010).
[16] J. P. Blaizot and J. Y. Ollitrault, Phys. Rev. Lett. **77**, 1703 (1996).

[17] A. Capella, L. Bravina, E. G. Ferreiro, A. B. Kaidalov, K. Tywoniuk, and E. Zabrodin, Eur. Phys. J. C **58**, 437 (2008).
[18] O. Linnyk, E. L. Bratkovskaya, and W. Cassing, Nucl. Phys. A **807**, 79 (2008).
[19] A. Andronic, P. Braun-Munzinger, K. Redlich, and J. Stachel, Nucl. Phys. A **789**, 334 (2007).
[20] R. L. Thews and M. L. Mangano, Phys. Rev. C **73**, 014904 (2006).
[21] L. Grandchamp, R. Rapp, and G. E. Brown, Phys. Rev. Lett. **92**, 212301 (2004).
[22] L. Yan, P. Zhuang, and N. Xu, Phys. Rev. Lett. **97**, 232301 (2006).
[23] X. Zhao and R. Rapp, Phys. Lett. B **664**, 253 (2008).
[24] C. Young and E. Shuryak, Phys. Rev. C **79**, 034907 (2009).
[25] S. Datta, F. Karsch, P. Petreczky, and I. Wetzorke, Phys. Rev. D **69**, 094507 (2004).
[26] A. Jakovac, P. Petreczky, K. Petrov, and A. Velytsky, Phys. Rev. D **75**, 014506 (2007).
[27] T. Umeda, Phys. Rev. D **75**, 094502 (2007).
[28] T. Umeda, PoS **LAT2007**, 233 (2007).
[29] P. Petreczky, Eur. Phys. J. C **62**, 85 (2009).
[30] L. Grandchamp and R. Rapp, Phys. Lett. B **523**, 60 (2001).
[31] T. Umeda and H. Matsufuru, Nucl. Phys. Proc. Suppl. **140**, 547 (2005).
[32] M. E. Peskin, Nucl. Phys. B **156**, 365 (1979); G. Bhanot and M. E. Peskin, *ibid.* **156**, 391 (1979).
[33] B. L. Combridge, Nucl. Phys. B **151**, 429 (1979).
[34] Z. Lin and C. M. Ko, Phys. Rev. C **62**, 034903 (2000).
[35] K. L. Haglin and C. Gale, Phys. Rev. C **63**, 065201 (2001).
[36] G. T. Bodwin, E. Braaten, and G. P. Lepage, Phys. Rev. D **51**, 1125 (1995); **55**, 5853(E) (1997).
[37] J. Huefner and P. F. Zhuang, Phys. Lett. B **559**, 193 (2003).
[38] N. S. Topilskaya *et al.* (NA50 Collaboration), Nucl. Phys. A **715**, 675 (2003).
[39] A. Adare *et al.* (PHENIX Collaboration), Phys. Rev. C **77**, 024912 (2008).
[40] C. W. De Jager, H. De Vries, and C. De Vries, Atom. Data Nucl. Data Table **14**, 479 (1974).
[41] I. Abt *et al.* (HERAB Collaboration), Phys. Lett. B **638**, 407 (2006).
[42] A. Adare *et al.* (PHENIX Collaboration), Phys. Rev. Lett. **98**, 232002 (2007).
[43] R. Arnaldi *et al.* (NA60 Collaboration), arXiv:1004.5523 [nucl-ex].
[44] B. Alessandro *et al.* (NA50 Collaboration), Eur. Phys. J. C **48**, 329 (2006).
[45] A. Frawley, talk at CATHIE INT Mini-Program on "Quarkonium in Hot Media: from QCD to Experiment," Seattle, WA, June 16–26, 2009 [http://www.int.washington.edu/talks/WorkShops/int_09_42W/].
[46] E. G. Ferreiro, F. Fleuret, J. P. Lansberg, and A. Rakotozafindrabe, Phys. Rev. C **81**, 064911 (2010).
[47] C. Lourenco and H. K. Wohri, Phys. Rept. **433**, 127 (2006).
[48] A. Adare *et al.* (PHENIX Collaboration), Phys. Rev. Lett. **97**, 252002 (2006).
[49] Y. F. Zhang, J. Phys. G **35**, 104022 (2008).
[50] P. Braun-Munzinger, K. Redlich, and J. Stachel, arXiv:nucl-th/0304013.
[51] M. Cheng *et al.*, Phys. Rev. D **74**, 054507 (2006).
[52] I. Arsene *et al.* (BRAHMS Collaboration), Nucl. Phys. A **757**, 1 (2005).
[53] X. Zhao and R. Rapp, Eur. Phys. J. C **62**, 109 (2009).
[54] J. Cleymans, K. Redlich, and E. Suhonen, Z. Phys. C **51**, 137 (1991).
[55] M. I. Gorenstein, A. P. Kostyuk, H. Stoecker, and W. Greiner, Phys. Lett. B **509**, 277 (2001).
[56] W. M. Yao *et al.* (Particle Data Group), J. Phys. G **33**, 1 (2006).
[57] L. Grandchamp and R. Rapp, Nucl. Phys. A **709**, 415 (2002).
[58] V. Greco, C. M. Ko, and R. Rapp, Phys. Lett. B **595**, 202 (2004).
[59] H. van Hees, M. Mannarelli, V. Greco, and R. Rapp, Phys. Rev. Lett. **100**, 192301 (2008).
[60] H. van Hees, V. Greco, and R. Rapp, Phys. Rev. C **73**, 034913 (2006).
[61] U. Heinz (private communication).
[62] S. Hamieh, K. Redlich, and A. Tounsi, Phys. Lett. B **486**, 61 (2000).
[63] S. A. Klinksiek, arXiv:hep-ex/0609002.
[64] R. Rapp and H. van Hees, in *Quark-Gluon Plasma 4*, edited by R. Hwa and X. N. Wang (World Scientific, Singapore, 2010), pp. 111–206.
[65] X. Zhao and R. Rapp (in preparation, 2010).
[66] E. Schnedermann, J. Sollfrank, and U. W. Heinz, Phys. Rev. C **48**, 2462 (1993).
[67] R. Rapp, Eur. Phys. J. C **43**, 91 (2005).
[68] L. Ramello *et al.* (NA50 Collaboration), Nucl. Phys. A **715**, 243 (2003).
[69] B. Alessandro *et al.* (NA50 Collaboration), Eur. Phys. J. C **39**, 335 (2005).
[70] A. Adare *et al.* (PHENIX Collaboration), Phys. Rev. Lett. **98**, 232301 (2007).
[71] R. Arnaldi (private communication).
[72] M. C. Abreu *et al.* (NA50 Collaboration), Phys. Lett. B **499**, 85 (2001).
[73] A. Adare *et al.* (PHENIX Collaboration), Phys. Rev. Lett. **101**, 122301 (2008).
[74] B. I. Abelev *et al.* (STAR Collaboration), Phys. Rev. C **80**, 041902 (2009).
[75] F. Karsch and R. Petronzio, Z. Phys. C **37**, 627 (1988).
[76] J. P. Blaizot and J. Y. Ollitrault, Phys. Rev. D **39**, 232 (1989).
[77] Z. Xu (private communication).
[78] X. Zhao and R. Rapp, arXiv:0806.1239 [nucl-th].